

Electronic Structure of a Chain-like Compound: TlSe

Ş. Ellialtıoğlu,* E. Mete,† R. Shaltaf

Department of Physics, Middle East Technical University, Ankara 06531, Turkey

and

K. Allakhverdiev,^{1,2} F. Gashimzade,¹ M. Nizamettinova,³ G. Orudzhev³

¹Institute of Physics, Azerbaijan National Academy of Sciences, Baku 370073, Azerbaijan

²Materials and Chemicals Technologies Research Institute, MAM, TÜBİTAK, Gebze/Kocaeli, Turkey

³Azerbaijan Technical University, Baku, Azerbaijan

(Dated: November 5, 2018)

An ab-initio pseudopotential calculation using density functional theory within the local density approximation has been performed to investigate the electronic properties of TlSe which is of chain-like crystal geometry. The energy bands and effective masses along high symmetry directions, the density of states and valence charge density distributions cut through various planes are presented. The results have been discussed in terms of previously existing experimental and theoretical data, and comparisons with similar compounds have been made.

PACS numbers: 71.15.Mb, 71.20.-b, 71.18+y

I. INTRODUCTION

Thallium selenide is a III–VI compound with body-centered-tetragonal (*bct*) structure of D_{4h}^{18} ($I4/mcm$) space group.¹ The quasi-one-dimensional nature² of its structure makes TlSe a generic example for a series of similar binary and ternary chain-like compounds with the formula unit of $Tl^+(Tl^{3+}Se_2^{2-})^-$ where for the ternary compounds monovalent and trivalent cations are of different atoms like in $TlInSe_2$, $TlGaTe_2$, and $TlInTe_2$. The trivalent Tl^{3+} ions are surrounded by four tetrahedrally bonded Se^{2-} ions. These tetrahedra share edges to form long negatively charged chains of $(Tl^{3+}Se_2^{2-})^-$ units that are parallel to *z*-axis coinciding with the optical *c*-axis (see Fig. 1). Monovalent Tl^+ ions on the other hand are surrounded by eight octahedrally positioned Se^{2-} ions, and they electrostatically hold these chains together by means of ionic inter-chain forces that are weaker than the intra-chain bonds of $Tl^{3+}-Se^{2-}$ which are ionic-covalent in nature. This leads to easy cleavage of TlSe-type crystals into plane parallel mirror-like plates along *c*-axis. As a result one has a “natural” (110) plane with mirror-like surface that is particularly useful for optical measurements and device applications. Also for the same reasons these crystals are highly anisotropic in many physical properties which consequently are enhanced under the influence of high pressures.^{3,4,5} In addition, the spin-exchange coupling between Tl^+ and Tl^{3+} ions is observed to be stronger⁶ as compared to the intra-chain couplings of the same nature between Tl^{n+} and Tl^{n+} ions.

The unit cell contains 8 atoms with atomic positions of two Tl^{3+} ions at $\pm(0, 0, c/4)$, two Tl^+ ions at $\pm(a/2, 0, c/4)$ and four Se^{2-} ions at $\pm(\eta a/2, \eta a/2, c/2)$ and $\pm(\eta a/2, -\eta a/2, 0)$, where η is the internal parameter. The primitive translation vectors are $(-a/2, a/2, c/2)$, $(a/2, -a/2, c/2)$ and $(a/2, a/2, -c/2)$. The lattice constants for TlSe can be found in the literature^{1,2} as $a=b=8.02\pm0.01$ Å and $c=7.00\pm0.02$ Å with the internal pa-

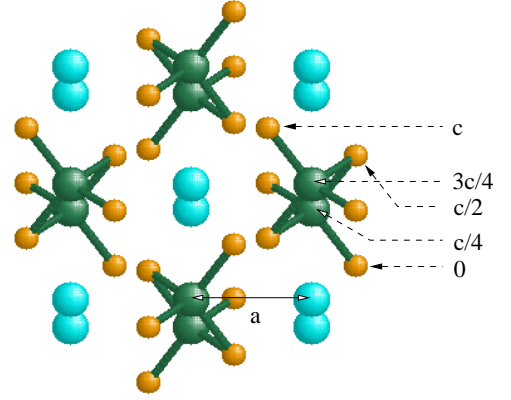


FIG. 1: Crystal structure of TlSe. Thallium atoms are represented by larger spheres and selenium atoms by smaller ones in order to emphasize the chains for better visualization. Se^{2-} ions are tetrahedrally bonded to Tl^{3+} ions forming chains of edge-sharing-tetrahedra, along *c*-axis. The Tl^+ ions are the spheres with no bonds shown.

rameter $\eta=0.358$.

The covalent bond between trivalent thallium and the divalent selenium is of length $d(Tl^{3+}-Se^{2-})=2.68$ Å, being just a little larger than the sum of the covalent radii, 1.48 Å and 1.16 Å, respectively. The length of ionic bond between the monovalent thallium placed in an octahedron of divalent selenium ions is $d(Tl^+-Se^{2-})=3.428$ Å, which is smaller than but close to the sum of the respective ionic radii⁷ of 1.59 Å and 1.98 Å. Other typical bond lengths are $d(Tl^{n+}-Tl^{n+})=3.5$ Å, $d_1(Se^{2-}-Se^{2-})=3.853$ Å, $d(Tl^{3+}-Tl^+)=4.01$ Å and $d_2(Se^{2-}-Se^{2-})=4.06$ Å.

It has been shown that TlSe-type crystals are promising materials in device applications as near- and far-infrared sensors, pressure sensitive detectors⁸ and as γ -ray detectors.⁹ Switching phenomena¹⁰ and low-temperature metallic conductivity¹¹ in TlSe have been

described successfully.

The energy band gap published by different authors are not in accordance and varies between 0.6 to 1.0 eV at 300 K.^{12,13} Band structure calculations and comparisons with the existing experimental data showed that TlSe-type materials are indirect gap materials; and the direct transitions are forbidden according to the symmetry selection rules.¹³ Electronic band structures of TlSe and related crystals were obtained by various groups and available in the literature.^{13,14,15,16,17,18,19}

Thallium selenide-type crystals possess a three dimensional electronic nature in spite of their chain-like crystal structure. But still the direction normal to the chains shows stronger band dispersion and consequently may be more conductive. This can be seen from the experimental values¹³ of direct and indirect gaps for different polarization directions. The direct gap is measured as 0.99 eV when the polarizations of the electric-field vector of the incident electromagnetic wave \mathbf{E} is normal to the optical c -axis (z -axis) whereas when \mathbf{E} is parallel to c -axis it is measured to be 1.05 eV. Similarly, the indirect gap values are observed to be 0.68 eV and 0.72 eV, respectively for the normal and parallel fields.

Effect of pressure and temperature on the electronic band structure of TlSe was first reported by Gashimzade and Orudzhev,³ and phase transitions in TlSe-type crystals under pressure were reviewed by Allakhverdiev and Ellialtıoğlu.^{4,5}

In the present work the results of an *ab-initio* pseudopotential calculations using density functional theory within the local density approximation for the electronic band structure as well as the density of states of TlSe are presented. In addition, the valence charge density distributions for various atomic planes are calculated. Effective masses for various valleys in different symmetry directions were estimated by using curvature fit to the bands. All these results are compared with the experimental and other theoretical values available.

II. METHOD

We have used a pseudopotential method based on density functional theory in the local density approximation. The self-consistent norm-conserving pseudopotentials are generated by using the Troullier-Martins scheme²⁰ which is included in the fhi98PP package.²¹ Plane waves are used as a basis set for the electronic wave functions. In order to solve the Kohn-Sham equations,²² conjugate gradients minimization method²³ is employed as implemented by the ABINIT code.²⁴ The exchange-correlation effects are considered using the Perdew-Wang scheme²⁵ as parametrized by Ceperley and Alder.²⁶

Pseudopotentials are generated using the following electronic configurations: for Tl, in addition to the true valence states ($6s$ and $6p$), $5d$ semicore states are also included in the calculation. For Se, $4s$ semicore and $4p$ true valence states are treated as valence states. The op-

timized calculation has produced the lattice parameters to be $a=b=7.91$ Å and $c=6.90$ Å, both of which are close to their experimental values within $\sim 1.4\%$.

Good convergence has been obtained for the bulk total energy calculation with the choice of a kinetic energy cut-off at 20 Ha for TlSe. In the density of states calculations the irreducible Brillouin zone (BZ) was sampled with 80 k -points using the Monkhorst-Pack²⁷ scheme.

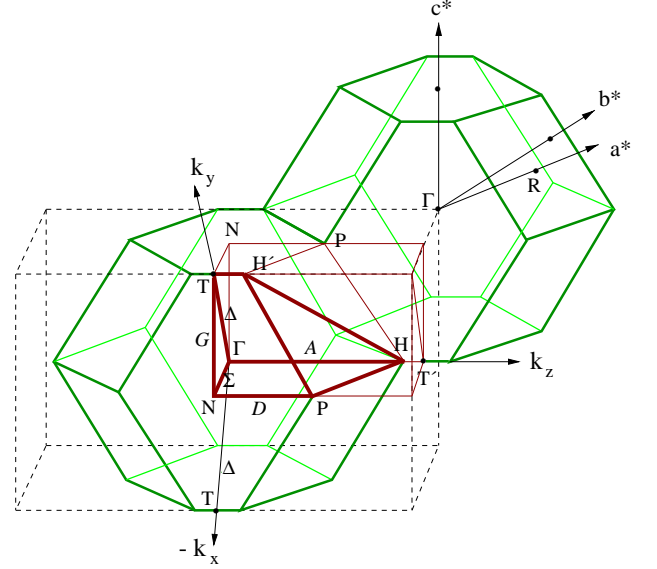


FIG. 2: The irreducible wedge (heavy lines) of the first Brillouin zone for TlSe structure with the high symmetry points and high symmetry lines indicated.

III. RESULTS AND DISCUSSION

The first Brillouin zone for TlSe in the bct structure is given in Fig. 2 where the high symmetry points and high symmetry lines are indicated on the irreducible part (1/16th) of the BZ and they are given by:

$R=(0, \pi/a, \pi/c)$, $P=(\pi/a, \pi/a, \pi/c)$, $N=(\pi/a, \pi/a, 0)$, $\Gamma=(0, 0, 0)$, $T=(0, 2\pi/a, 0) \equiv T'=(0, 0, 2\pi/c)$ and $H=(0, 0, (1+u^2)\pi/c) \equiv H'=(0, 2\pi/a, (1-u^2)\pi/c)$ where $u = c/a$. Symmetry lines of the Brillouin zone: $K=(k, \pi/a, \pi/c)$, $D=(\pi/a, \pi/a, k)$, $\Sigma=(k, k, 0)$, $\Delta=(0, k, 0)$, $A=(0, 0, k)$ and $G=(k, 2\pi/a-k, 0)$.

The dashed box in Fig. 2 has edges of $\sqrt{2}(2\pi/a) \times \sqrt{2}(2\pi/a) \times 2(2\pi/c)$, the corners of which are the centers (Γ') of neighboring Brillouin zones. Similarly, the point H' is equivalent to H since it is the H -point of the neighboring BZ. The reciprocal lattice vectors for our choice of primitive translation vectors are given by $\mathbf{G}_1=(0, 2\pi/a, 2\pi/c)$, $\mathbf{G}_2=(2\pi/a, 0, 2\pi/c)$ and $\mathbf{G}_3=(2\pi/a, 2\pi/a, 0)$ along \mathbf{a}^* , \mathbf{b}^* and \mathbf{c}^* axes, respectively.

The energy bands calculated for the \mathbf{k} -points along the high symmetry lines are shown in Fig. 3. Also shown in the four rightmost panels are the total density of states

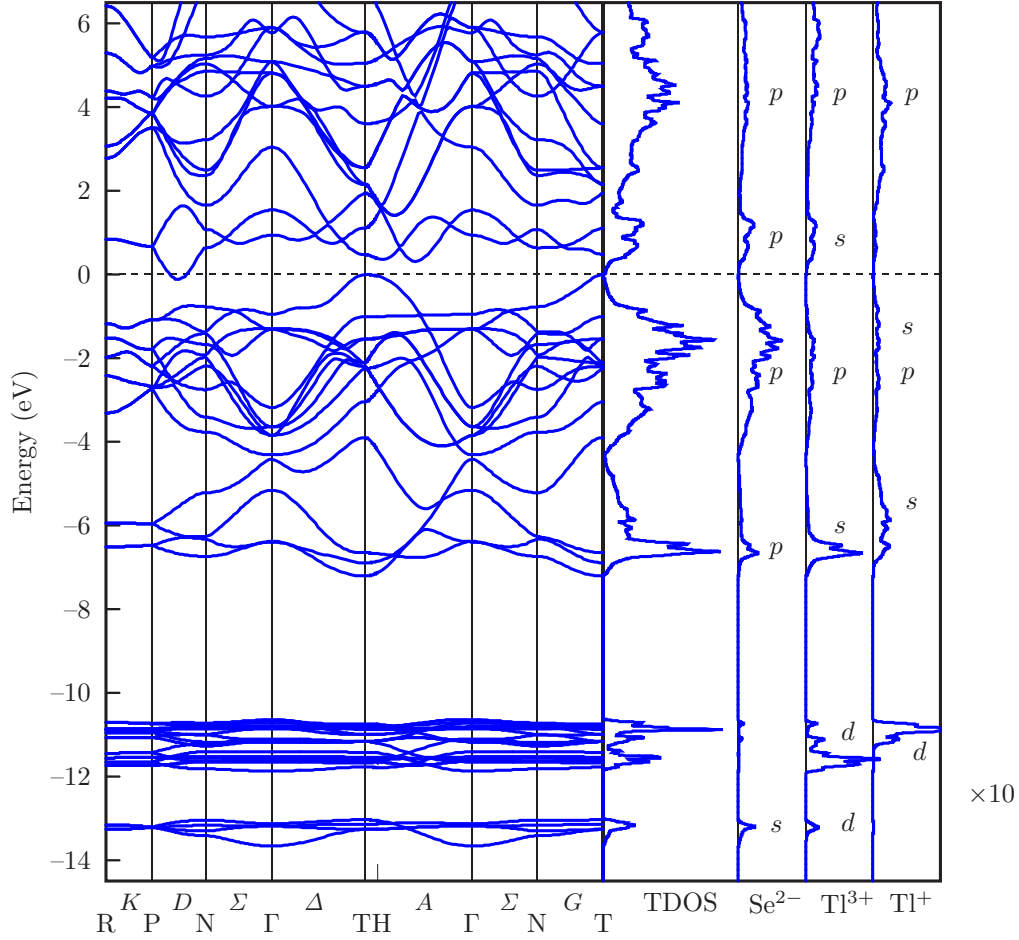


FIG. 3: The energy bands for TlSe along the high symmetry lines of the Brillouin zone, the corresponding total density of states, and the local densities of states for the Se^{2-} , Tl^{3+} , and Tl^+ , in panels from left to right, respectively. The densities of states for the lower valence (semi-core) states due to Tl $5d$ and Se $4s$ electrons are shown in a scale ten times smaller than the rest of the densities above -9 eV. The top of the valence band is taken to be zero.

for the TlSe compound, as well as the local densities of states for the individual ions, Se^{2-} , Tl^{3+} , and Tl^+ , respectively.

At the bottom of the figure there are 4 bands originated from $4s$ states of the Se atoms located in the range 13 to 13.7 eV below the top of the valence band, which is chosen as zero. Above this group there are 20 bands consisted of $5d$ states of Tl atoms located in the range from -10.6 to -12 eV, and being semicore d -states they are not much dispersed in most \mathbf{k} -directions, except a little along D , and along A .

In the region between -4 and -7 eV, there is an isolated group of 4 bands which are made up of mostly the $6s$ states of monovalent Tl ion, and some Se $4p$ states at the bottom of the valence band mixed with the $6s$ states of trivalent cation. Another group consisting 10 bands in the upper part of the valence band is mainly due to Se $4p$ -states and $6p$ states of both Tl atoms. However, the uppermost valence band which tops at the symmetry point T is composed of mainly nonbonding Se $4p$ and $6s$ states of monovalent Tl.

The 2 bands in the lower part of the conduction bands are the antibonding mixture of the Se $4p$ -states with the $6s$ states of Tl^{3+} , and intermixed only slightly (around H) with the 12 upper conduction bands that are located above ~ 1.5 eV, and made up of p -states of all three ions.

All of the bands along the line K joining R and P points are doubly degenerate due to time reversal symmetry.¹⁵

The bottom of the conduction band is located almost at the midway $D_1 = (\pi/a, \pi/a, \pi/2c)$, along the line D joining the points P and N, and corresponds to the irreducible representation D_1 . Two additional minima are situated along the symmetry line A which connects the points Γ and H, one very close to the midway (A_4) and the other is very close to the point H. The band at point T is a little higher in energy.

The top of the valence band is sharply defined and located at the high symmetry point T which corresponds to the irreducible representation T_3 . The $T_3 \rightarrow T_4$ vertical transition is forbidden in the dipole approximation, however, minimal direct transition is allowed at point H (near T along A). The bottom of the valence bands is

also at the symmetry point T with s -like minimum, and the valence band width is found to be 7.21 eV.

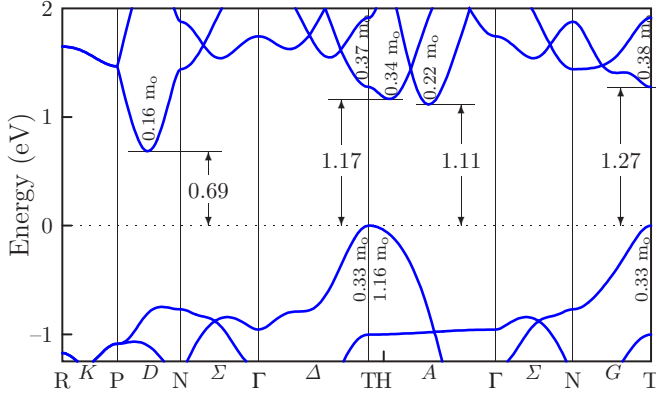


FIG. 4: Energy gap values and effective masses for valleys along various directions. The conduction bands are rigidly shifted upward in energy by a fixed amount of 0.8 eV (see the text)

The energy gap is underestimated relative to the experimental value due to the well known artifact of the LDA calculations,²⁸ as a result that the indirect gap appears to be negative which instead should be about 0.7 eV. Note that the similar deficiency is observed by Okazaki et al.¹⁸ for the semiconductor TlGaTe₂ using ab-initio LAPW method, and resulting to a band structure with slightly negative gap also, leading to a semimetal with hole pocket at T₃ and electron pocket at D₁. Hence, for a rough correction, if the whole conduction band (of 14 states) as a block is rigidly shifted upwards by 0.8 eV to arrive at the indirect gap value (0.69 eV seen in Fig. 4) of TlSe then a direct gap of 1.27 eV is obtained as a consequence, which is to be compared with the experimental value of roughly 1.0 eV.¹³ The other indirect gaps will then be seen as 1.11 eV for the valley along A and 1.17 eV for the valley along the same direction but just a few meV's away from H-point. The curvature of the lowest conduction band along TH has the same sign but is larger than that of the highest valence band along the same edge of the BZ, and thus the vertical gap at H-point being 1.22 eV is 0.05 eV smaller than the direct gap at T-point where the valence band top is located.

From the curvatures of bands the effective masses are obtained by linear fitting of E versus k^2 plots at the close proximity of the extrema. They are shown in Fig. 4 for different valleys in units of free electron mass m_0 . The hole effective masses along Δ and Σ are found to be very close to each other being $m_h^*(T_3) = 0.33 m_0$, however, along TH it is as high as $m_h^*(T_3) = 1.16 m_0$ and increasing curvature after H along A reduces it to $0.61 m_0$ (at H) giving rise to a combined value of $0.81 m_0$ at T. The electron effective masses at T along Δ and Σ are again similar and have values of $m_e^*(T_4) = 0.37 m_0$ and $0.38 m_0$, respectively. Along TH the curvature of this band is opposite of those along Δ and G causing T₄ to be a saddle point as is well-known. Other valleys along

A correspond to effective masses of $0.34 m_0$ and $0.22 m_0$ as seen in Fig. 4 and the electron effective mass for the lowest minimum along D is found to be $0.16 m_0$. The experimental values obtained from conductivity and Hall effect measurements²⁹ are $m_e^* = 0.3 m_0$ and $m_h^* = 0.6 m_0$ and from thermoelectric measurements³⁰ is $m_h^* = 0.86 m_0$.

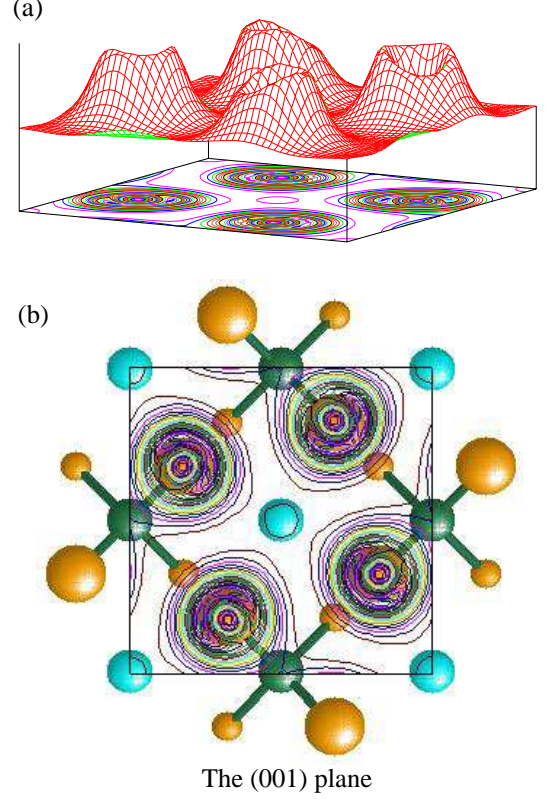


FIG. 5: (a) Oblique surface plots and (b) top views of the total valence charge density contours for TlSe cut through the top (001) plane containing the Se²⁻ ions (larger balls). Tl ions (medium balls) and half of the Se ions (smallest balls) are in (004) and (002) planes, respectively.

The total valence charge densities for different planes of atoms were calculated to show the charge transfer which are in accordance with the local density of states results in identifying the electronic structure of the compound. Fig. 5 shows the plot for the (001) plane which cuts through the Se²⁻ ions at positions $\pm(\eta a/2, -\eta a/2, 0)$. The bottom plane of (002) containing the other Se²⁻ pair of the same tetrahedron gives the same charge density plot, except it is flipped in x - or y -axis.

Fig. 6 shows the case for the (004) plane that contains Tl³⁺ ions at $\pm(0, 0, c/4)$ and Tl¹⁺ ions at $\pm(a/2, 0, c/4)$. Tl¹⁺ ions having been stripped from their $6p$ electron show their s -like character due to the outermost $6s^2$ electrons participating in the valence bands. This can also be seen in the energy band picture as rather quadratic (s -like) minimum and maximum at the high symmetry point T (see Fig. 3). Donated their $6p$ and $6s$ electrons to bond formation, Tl³⁺ ions, on the other

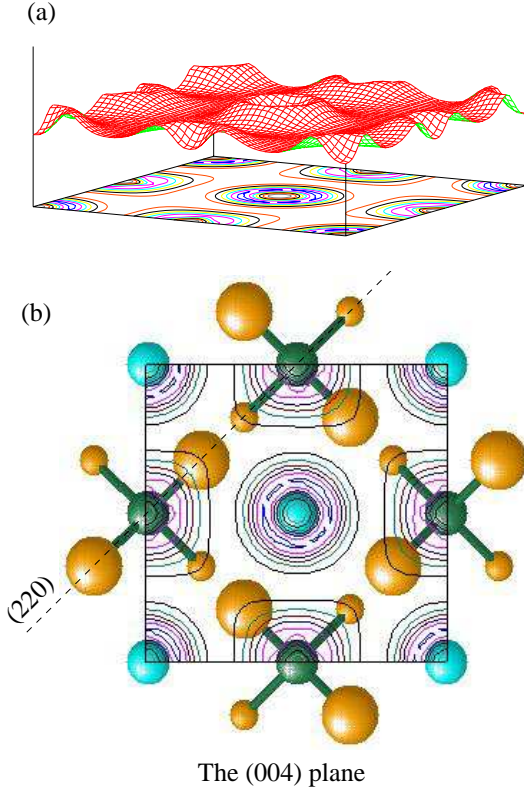


FIG. 6: (a) Oblique surface plots and (b) top view of the total valence charge density contours for TlSe cut through the (004) plane containing both Tl^+ (center and corners) and Tl^{3+} (edges) ions. Se^{2-} ions shown are not in plane, but either above (larger balls) or below (smaller balls) by $c/4$.

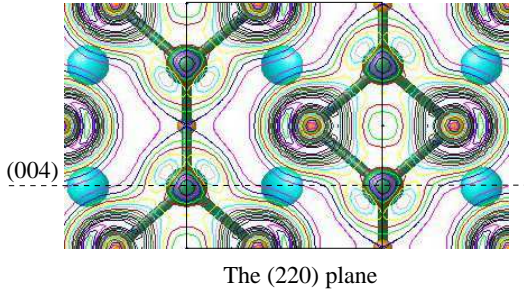


FIG. 7: Contour plots of the total valence charge density for TlSe cut through the (220) plane containing Tl^{3+} and Se^{2-} ions. Tl^+ ions shown are not in plane. The frame shows the part of (220) plane inside the cube shown in Fig. 6

hand, show some charge density extending towards Se^{2-} ions and a negligible amount of d -influence in Fig. 6(b).

These findings can only be roughly compared with the earlier empirical calculations³¹ since the charge density contours for (001), (002) and (004) planes were superimposed in one plot and the amplitude variations along the bonds were depicted in a different figure. Therefore, in order to compare the pronounced charge accumulation at the $\text{Tl}^{3+}\text{-Se}^{2-}$ bonds found in the empirical calcula-

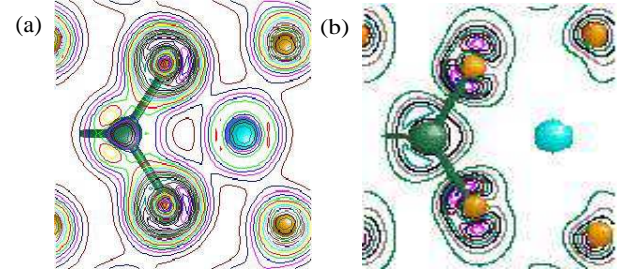


FIG. 8: Contour plots of, (a) the total valence charge density and (b) the charge density due to the lowest two conduction bands, for TlSe cut through an incommensurate plane containing all three ions.

tion, charge density distribution on two other planes both passing through these bonds are also presented. Fig. 7 shows the total valence charge density plots for the (220) plane that passes through the $\text{Tl}^{3+}\text{-Se}^{2-}$ bonds, where most of the charge is seen to be accumulated on the Se^{2-} ion rather than on the bond. The second plane that contains the bonds under consideration contains also the monovalent cation. The total valence charge density calculated for this plane is shown in Fig. 8(a), where the monovalent cation is seen to be not bonded to the chalcogen ions. Again the $\text{Tl}^{3+}\text{-Se}^{2-}$ bond is seen to be more ionic than covalent in nature. Finally, Fig. 8(b) shows the same plane that contains all three ions as (a), however, this time the charge density contours depict the contributions from the lowest two conduction bands only. It is clearly seen that the monovalent cation has no electron at these antibonding bands which are formed by Tl^{3+} 6s and Se^{2-} 4p states alone, consistent with the rightmost panel in Fig. 3.

IV. SUMMARY AND CONCLUSION

Ab-initio pseudopotential calculations using density functional theory within the local density approximation has been performed for the first time to investigate the electronic properties of TlSe. The energy bands along different symmetry directions, the local and total densities of states, and total valence charge density distributions for certain plane-cuts are presented.

It is shown that the top of the valence band is sharply defined and located at the high symmetry point T, which corresponds to the irreducible representation T_3 . The bottom of the conduction band is located almost at the midway $(\pi/a, \pi/a, \pi/2c)$ between symmetry points P and N, along the the line D , and corresponds to the irreducible representation D_1 .

The distribution, dispersion and the orbital characters of the bands are in good agreement with the experimental data of the photoemission.³² The only prior band structure calculation for TlSe is reported by Gashimzade et al.¹⁵ where they have used a model pseudopotential and applied an empirical method. Although there is a general

agreement between the two results, there are some major differences as well. In their result there is an isolated group consisted of the top 2 valence bands which does not appear separated from the rest of the valence band in our calculations. And the isolated group of 4 bands at the bottom of the valence band in our calculations is not separated from the rest of the valence band in their results. Moreover, the order of their bands at the symmetry point N does not agree for most bands with that of the present results. These differences arise from the fact that Gashimzade et al.¹⁵ used restricted number of plane waves in their empirical pseudopotential method, and moreover, the wave functions were not deconvoluted enough. It is known that in such approximations it is not possible to take into account the screening, and to include the electron-ion interaction as well as the exchange-correlation effects properly. Another difference with this study is, although they have included the 4s semicore states of Se atoms, the 5d states of Tl atoms were not taken into account in their calculations. To single out the effect of *d* states, we have made separate calculations with and without including the 5d semicore states of Tl. Upon inclusion of *d* states the main change was on the 4s semicore states of Se which got narrowed down from dispersion between -13.7 eV to -12.2 eV to -13.7 eV to -13 eV, decreasing the bandwidth from 1.4 eV to 0.7 eV. The other change occurred in the lowest two conduction bands that are shifted downward and separated from the rest of the conduction bands by about 0.2 eV in all sym-

metry directions.

It is worth noting here that a similar electronic band structure for TlInSe₂ is obtained from a calculation¹⁹ made by constructing the pseudopotentials using the scheme suggested by Bachelet et al.³³ Although it is a semiconductor with a direct gap, valence band structure is qualitatively analogous to that of TlSe presented here. Isolation of the group of lowest 4 valence bands, the shape of the highest valence band, especially along the Γ TH Γ symmetry directions, and sharpness of the valence band top are their similar behavior. Another material to be compared is the TlGaTe₂, ab-initio band structure of which has been published by Okazaki et al.¹⁸ Not mentioning the quantitative differences, in general, the two band structures are remarkably similar, apart from some variations in the vicinity of Γ point of the Brillouin zone.

Acknowledgments

This work was supported by TÜBİTAK, The Scientific and Technical Research Council of Turkey, Grant No. TBAG-2036 (101T058).

* Corresponding author. Email: sinasi@metu.edu.tr

† Permanent address: Balıkesir Üniversitesi, Fizik Bölümü, Balıkesir 10100, Turkey.

-
- ¹ J. A. Ketelaar, W. H. t'Hart, M. Moerel, and D. Polder, *Z. Kristallogr.* **A101**, 396 (1939).
 - ² R. W. G. Wyckoff, "Crystal Structures", 2nd edition, Vol. **2**, (Interscience, New York, N. Y., 1964).
 - ³ F. M. Gashimzade and G. S. Orudzhev, *Phys. Stat. Solidi (b)* **106**, K67 (1981).
 - ⁴ K. R. Allakhverdiev and Ş. S. Ellialtıoğlu, *Frontiers of High Pressure Research II: Application of High Pressure to Low-Dimensional Novel Electronic Materials*, Kluwer Academic Publishers, NATO Science Series II: Mathematics, Physics and Chemistry **48**, 119 (2001).
 - ⁵ K. R. Allakhverdiev, T. G. Mamedov, B. G. Akınoğlu, and Ş. S. Ellialtıoğlu, *Tr. J. Phys.* **18**, 1 (1994).
 - ⁶ A. M. Panich and N. M. Gasanly, *Phys. Rev. B* **63**, 195201 (2001).
 - ⁷ R. D. Shannon, *Acta Cryst.* **A32**, 751 (1976).
 - ⁸ K. R. Allakhverdiev, Sh. G. Gasymov, T. G. Mamedov, M. A. Nizamettinova, and E. Yu. Salaev, *Sov. Phys. Semicond.* **17**, 131 (1983).
 - ⁹ S. G. Abdinova and I. V. Alekseev, *Nucl. Instr. and Mater. in Phys. Res.* **A411**, 365 (1998).
 - ¹⁰ B. Abay, B. Gürbulak, M. Yıldırım, H. Efeoglu, and Y. K. Yoğurtçu, *Phys. Stat. Solidi (a)* **153**, 145 (1996).
 - ¹¹ N. A. Abdullaev, M. A. Nizamettinova, A. D. Sardarly, and R. A. Süleymanov, *J. Phys.: Condensed Matter* **4**, 10361 (1992), [*Fiz. Tverd. Tela* **35**, 77 (1993)], *Phys. Solid State* **35**, 41 (1993).
 - ¹² E. Mooser and W. B. Pearson, *J. Electron* **1**, 629 (1956).
 - ¹³ R. S. Itoga and C. R. Kannewurf, *J. Phys. Chem. Solids* **32**, 1099 (1971).
 - ¹⁴ F. M. Gashimzade and G. S. Orudzhev, *Dokl. AN Azerb. SSR*, **36**, 18 (1980).
 - ¹⁵ F. M. Gashimzade, G. S. Orudzhev, [*Fiz. Techn. Poluprovodn.* **15**, 1311 (1981)], *Sov. Phys. Semicond.* **15**, 757 (1981).
 - ¹⁶ L. L. Janulionis, G. A. Bobonas, M. A. Nizamettinova, G. S. Orudzhev, A. Ju. Shilejka, *Proceedings Lithuanian Physical Society (in Russian)* **22**, 63 (1982).
 - ¹⁷ D. G. Kilday, D. W. Niles, and G. Margaritondo, *Phys. Rev. B* **35**, 660 (1987).
 - ¹⁸ K. Okazaki, K. Tanaka, J. Matsuno, A. Fujimori, L. F. Mattheiss, S. Iida, E. Kerimova and N. Mamedov, *Phys. Rev. B* **64**, 045210 (2001).
 - ¹⁹ G. Orudzhev, N. Mamedov, H. Uchiki, N. Yamamoto, S. Iida, H. Toyota, E. Gojaev, F. Hashimzade, *J. Phys. Chem. Solids* **64**, 1703 (2003).
 - ²⁰ N. Troullier and J. L. Martins, *Phys. Rev. B* **43**, 1993 (1991).
 - ²¹ M. Fuchs and M. Scheffler, *Comput. Phys. Commun.* **119**, 67 (1999).
 - ²² W. Kohn and L. J. Sham, *Phys. Rev.* **140**, 1133A (1965).
 - ²³ M. C. Payne, M. P. Teter, D. C. Allan, T. A. Arias, and J. D. Joannopoulos, *Rev. Mod. Phys.* **64**, 1045 (1992).
 - ²⁴ X. Gonze, J.-M. Beuken, R. Caracas, F. Detraux, M. Fuchs, G.-M. Rignanese, L. Sindic, M. Verstraete, G. Zerah, F. Jollet, M. Torrent, A. Roy, M. Mikami, Ph.

- Ghosez, J.-Y. Raty, and D. C. Allan. Computational Materials Science **25**, 478 (2002).
- ²⁵ J. P. Perdew and Y. Wang, Phys. Rev. B **45**, 13244 (1992).
- ²⁶ D. M. Ceperley and B. J. Alder, Phys. Rev. Lett. **45**, 566 (1980).
- ²⁷ H. J. Monkhorst and J. D. Pack, Phys. Rev. B **13**, 5188 (1976).
- ²⁸ R. O. Jones and O. Gunnarsson, Rev. Mod. Phys. **61**, 689 (1989).
- ²⁹ G. D. Guseinov, G. A. Akhundov, and G. B. Abdullaev, [Fiz. Tverd. Tela (Leningrad) **4**, 1206 (1962)], Phys. Solid State **4**, 885 (1962).
- ³⁰ S. A. Aliev, M. A. Nizametdinova, Sh. O. Orudzheva, and S. I. Tairov, [Fiz. Techn. Poluprovodn. **5**, 567 (1971)], Sov. Phys. Semicond. **5**, 499 (1971).
- ³¹ G. S. Orudzhev, Sh. M. Efendiev, and Z. A. Dzhakhagirov, [Fiz. Tverd. Tela **37**, 284 (1995)], Phys. Solid State **37**, 152 (1995).
- ³² L. Porte and A. Tranquard, J. Solid State Chem. **35**, 59 (1980).
- ³³ G. B. Bachelet, D. R. Hamann, and M. Schlüter, Phys. Rev. B **26**, 4199 (1982).